UNITED NATIONS **E/CONF.97/5/CRP. 5**

ECONOMIC AND SOCIAL COUNCIL

Seventeenth United Nations Regional Cartographic Conference for Asia and the Pacific
Bangkok, 18-22 September 2006
Item 6 (b) of the provisional agenda*

COUNTRY REPORTS

DETECTION OF CRUSTAL DEFORMATION OF THE NORTHERN PAKISTAN EARTHQUAKE BY SATELLITE DATA

Submitted by Japan **

*** E/CONF.97/1**

**** Prepared by Geographical Survey Institute of Japan.**

DETECTION OF CRUSTAL DEFORMATION OF THE NORTHERN PAKISTAN EARTHQUAKE BY SATELLITE DATA

Geographical Survey Institute
Kitasato-1, Tsukuba, Ibaraki 305-0811 JAPAN

Abstract

A large-scale earthquake with a magnitude of 7.6 occurred on October 8, 2005 in the northern part of Pakistan. The Geographical Survey Institute carried out various analyses to clarify the crustal deformation accompanied with the earthquake in detail with the data from the satellites.

We mapped the crustal deformation spatially with Synthetic Aperture Radar data from the European Space Agency's ENVISAT, and found that the newly deformed area occupies a 90-kilometer-long northwest-southeast trending strip. Heavily damaged area north of Muzaffarabad has the maximum deformation up to 6-meter uplift as observed by the satellite.

There are known active faults stretching to the northwest and southeast near the epicenter, which reveal some uplift (on the northeastern side) and dextral (right-lateral) strike-slip activities. The detected crustal deformation was along these active faults and all observations were consistent with previously known directions of past fault movements. Model calculations also showed that the faults slipped a maximum of about nine meters.

In addition, analysis using other high-resolution images from IKONOS and SPOT-5 satellites showed that slope failures occurred along the active faults and were concentrated on the northeastern side.

1. Introduction

The Northern Pakistan Earthquake (M 7.6) of October 8, 2005 occurred in the Kashmir region in the northwestern part of the Himalayas. The epicenter was north-northeast direction and 105 km away from Islamabad, capital city of Pakistan. According to the UN Office for the Coordination of Humanitarian Affairs, 73,331 were killed by the earthquake as of April 2006.

Despite the magnitude of damages, it was difficult to understand the overall features of this catastrophe; what kind of crustal movement occurred and where, what was the tectonic background, how the damages distributed spatially etc. because the earthquake occurred in mountainous remote area from the capital city and telecommunication network from affected area was seriously damaged by the earthquake.

The Geographical Survey Institute (GSI), a national surveying and mapping organization in Japanese Government, carried out various analyses to clarify the crustal deformation accompanied with the earthquake in detail with the data from satellites. The methods include Synthetic Aperture Radar (SAR) data analysis, fault model calculations and interpretation of high resolution satellite images. As the result, the satellite data have shown the ruptured earthquake faults in detail, allowing relief planners to quickly estimate the damaged areas and the extent of the damage for prompt rescue and relief operations.

2. SAR Data Analysis

SAR measures ground geometry and the distance between the satellite and the ground surface with radar waves. By compiling several successive radar pulses from a source

moving over a target, an image can be formed of that target that combines all the received echoes. In this study, earthquake deformation was found by comparing SAR data of the same region from European Space Agency's ENVISAT, one before the earthquake (17 September 2005) and one after (22 October 2005).

The ENVISAT data collected during this study are from descending acquisitions that result in an east-southeast line-of-sight (LOS) direction from the ground target to the satellite. The measured crustal deformation is the change in length along the radar LOS from the ground target to the SAR satellite. The components of displacement in each direction (north-south, east-west, and up-down) have not been directly determined.

Interferometric synthetic aperture radar (InSAR) from space, which calculates the pixel-by-pixel phase differences between two SAR images generated at different times over the same location, has become a powerful tool to monitor deformation of the Earth's surface because the technique has high measurement accuracy (a few centimeters).

We measured the displacement fields before and after the earthquake using InSAR. However, maps of displacement as calculated by InSAR were incoherent near the fault, mainly because of the high deformation gradients resulting from the large displacement (approximately several meters). Because the measured phase is only modulo 2π rad (half of the wavelength), the phase in the high deformation gradients area changes too rapidly to count the phase cycles; in other words, undersampling occurs. Furthermore, strong seismic motion near the fault caused a loss of coherence over the damaged area.

Therefore, we measured the displacement fields of the two SAR amplitude images taken before and after the earthquake using a sub-pixel-level offset estimation technique [Tobita et al., 2001]. Its measurement accuracy is lower (~1 meter) than that of InSAR, but it succeeded in detecting this

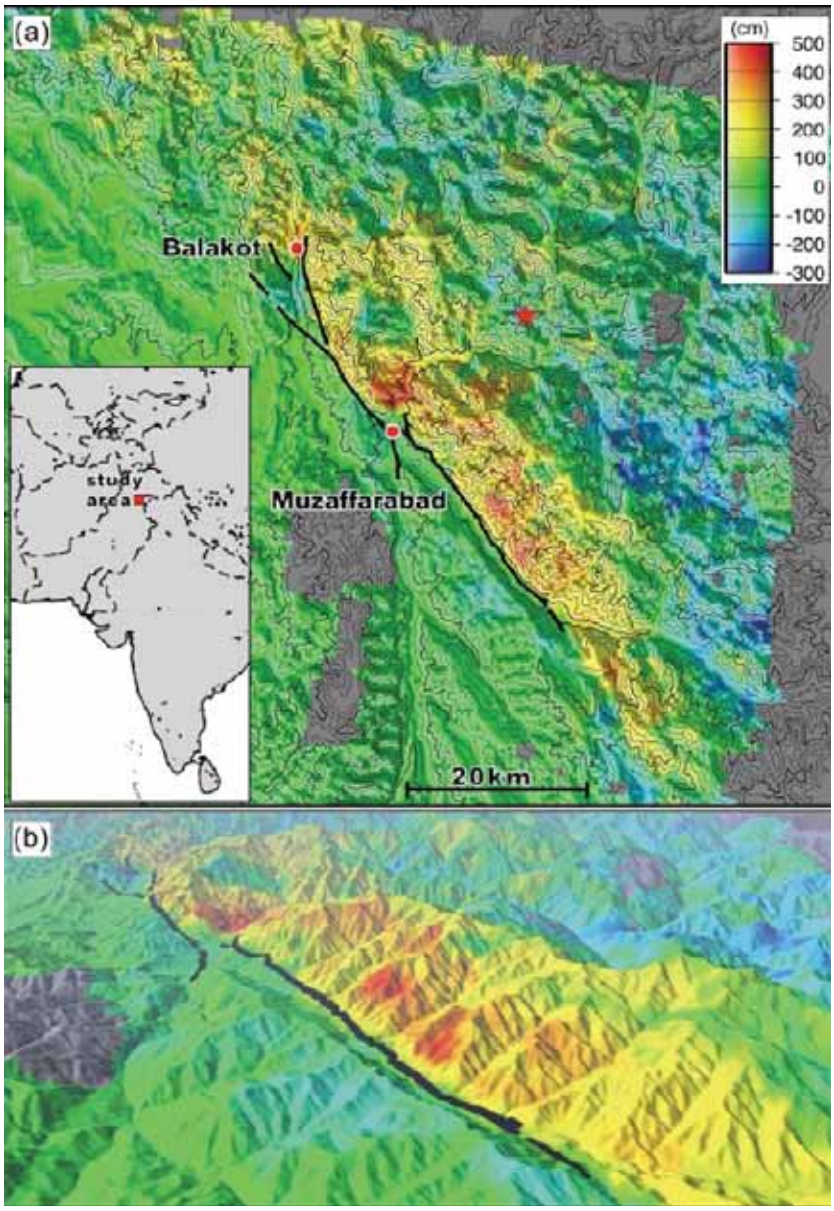

Fig.1 (a) Combined crustal deformation map superimposed on topography and the location of known active faults. Positive values indicate the movement of deformation, in centimeters, toward the SAR satellite in the LOS direction (upward and/or E-SE displacement). The red star shows the epicenter determined by the U.S. Geological Survey. The contour lines are every 250 meters generated by the NASA Shuttle Radar Topography Mission(SRTM). The black curves show the locations of active faults [Nakata et al., 1991].
(b) A bird's-eye view of crustal deformation and active faults (from the south).

deformation that is impossible to measure with InSAR. Figure 1(a) is a combination map of the InSAR and the SAR offset field analyses, and it shows several-meter-scale crustal deformations extending in a strip. In addition, it shows that the heavily-damaged area north of Muzaffarabad experienced about five meters of deformation.

3. Fault Modelling

A fault model was constructed to simulate the surface displacement of Figure 1a. Using a buried fault model in a homogeneous elastic half-space, as formulated by Okada [1985], the model fault was divided into three rectangular faults on which slip is uniform. Optimal fault parameters were estimated using an iterative least squares method. The estimated parameters are listed in Table 1, and positions of each fault plane are shown in Figure 2. The calculated moment magnitude is 7.6, which matches the U.S. Geological Survey estimated magnitude.

Table 1. Simulated Fault Parameters

Fault Position	*Latitude, °N*	*Longitude, °E*	*Depth, km*	*Length, km*	*Width, km*	*Strike, deg*	*Dip, deg*	*Rake, deg*	*Slip, m*
A	34.375	73.469	0.3	25	17	332	38	104	6.0
B	34.146	73.719	1.5	32	22	323	16	92	8.6
C	34.034	73.810	1.5	15	11	325	33	103	2.2

4. Active Faults and Displacement

Since most of the areas affected by the earthquake are in mountainous regions and access is prevented by slope failures that have blocked the roads, ground survey is limited. At the moment of our study, no surface fault rupture has been identified by ground survey. Therefore, locating the earthquake faults by SAR data was important. The active faults in Figures 1, 2, and 3 were identified prior to the earthquake by interpreting aerial photographs, and were determined from geomorphologic analysis to be reverse dextral strike-slip faults with uplift on the northeastern side [Nakata et al., 1991] (see also http://www.fal.co.jp/geog_disaster/20051018_pakistan.html). The crustal deformation detected by this study is along these active faults, and both methods used were consistent in predicting the type of fault displacement that occurred.

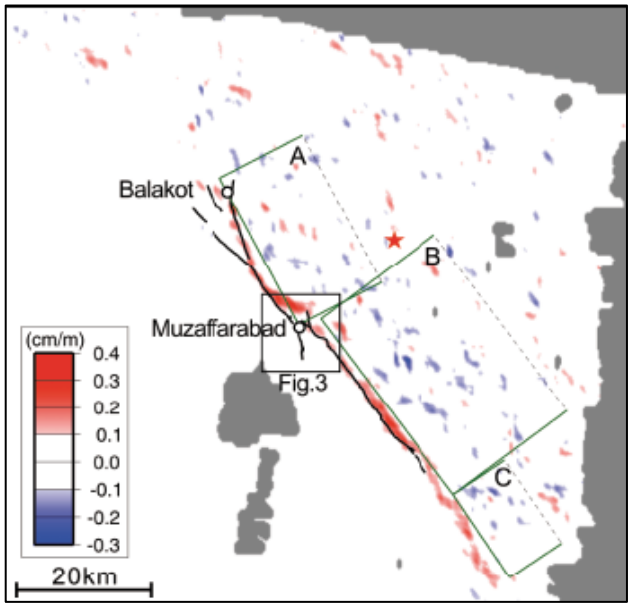

Fig. 2 Surface displacement gradient map in the northeast-southwest direction. The black curves show the locations of active faults. Rectangles A, B, and C are the calculated fault positions, and dashed lines show the deeper side of each fault. The red star shows the epicenter determined by the U. S. Geological Survey.

To estimate the position on the Earth's surface of the shallow side of the buried dipping faults, the surface displacement gradient [Fujiwara et al., 2000] was calculated in the northeast-southwest direction (Figure 2) using data from the SAR deformation image shown in

Figure 1(a). The large gradient area clearly coincides with the known active faults. Therefore, this earthquake is considered to have been generated by movement on these preexisting active faults. Additionally, it shows that fault movement also occurred in the southern extension of these active faults. Although there is a small discrepancy between the position of the shallow side of the simulated dipping faults and the area of the large displacement gradient, each extension of the buried shallow side to the surface generally agrees with the large gradient area. The rupture of northern fault plane 'A' approached closer to the surface than those of southern 'B' and 'C' (see Table 1). The known active faults are divided in two fault groups, the Muzaffarabad fault (northwest of Muzaffarabad) and the Tanda fault (southeast of Muzaffarabad) [Nakata et al., 1991]. These two faults run parallel near Muzaffarabad where the large gradient area in Figure 2 bends and transfers from the Muzaffarabad fault to the Tanda fault.

The observations reported here show that earthquakes in the regional tectonic stress field tend to occur at the same preexisting faults and have formed the topography. The SAR analysis also shows that the topography and active faults have a close correlation to the displacement (see Figure 1). In other words, coseismic deformation mimics the topography [Fujiwara et al., 2000]. It suggests that the known active faults are a result of accumulated fault movement over time.

5. Interpretation of IKONOS

We interpreted high-resolution optical satellite imagery to map the changes in topography, i.e. distribution of slope failures, surface displacement caused by the movement of earthquake faults, traces of liquefaction etc. (Figure 3). One-meter-resolution IKONOS images, which were taken on 22 September 2002 (before the earthquake) and 9 October 2005 (after the earthquake) are published on the Web (http:// www.spaceimaging.com/gallery/asiaEQViewer.htm). The area shown in Figure 3 is the

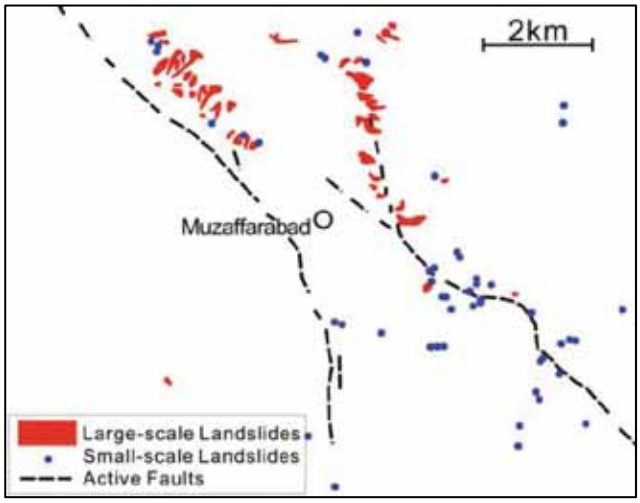

Fig. 3 Distribution of slope failures around Muzaffarabad, interpreted using IKONOS imagery.

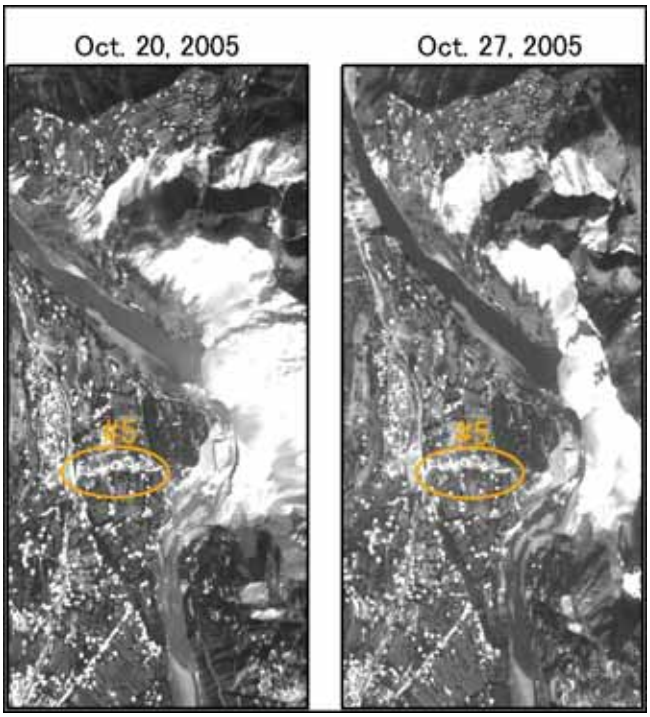

Fig.4 SPOT-5 stereo-imagery of the damaged area of north Muzaffarabad. The circle #5 indicates heavily damaged area along the surface rupture of an earthquake fault.

central part of Figure 1(a), around Muzaffarabad. The interpretation detected about 100 slope failures, most of which occurred along the active faults concentrated on the uplift side (northeast). Some large-scale slope failures were identified in the north and northwest of Muzaffarabad. These slope failures were located around a ~4-meter LOS earthquake displacement as seen by SAR; large-scale slope failures are not identified southeast of Muzaffarabad, where LOS displacement as seen by SAR is only about one meter. It is inferred that the large amount of uplift and/or strong seismic motion just over the fault triggered large-scale slope failures.

6. Distribution of Slope Failures Detected from SPOT-5

We obtained SPOT-5 panchromatic images taken on October 20 and 27, 2005, whose resolution is 2.5 meters. The incident angle of October 20 and 27 images is at the left side of 26.4 degree and at the right side of 30.4 degree, respectively. As shown in Figure 4, these images enable stereoscopic vision, and through the stereo-images slope failures were interpreted and delineated on the images. Figure 4 shows a part of north area of Muzaffarabad. In the figure the circle #5 shows not slope failures but the flexure cliff along the surface rupture of the earthquake fault.

Slope failures are interpreted as white-bright slope, especially the right side of the river. In delineating such the slope failure, each slope failure was divided as considering unit slope.

We have interpreted all the slope failures in the SPOT-5 images. The interpreted slope failures were overlaid on the SRTM data, and shown in Figure 5. The total count of the slope failures was 2,424. Many slope failures occurred along Muzaffarabad fault and Tanda fault.

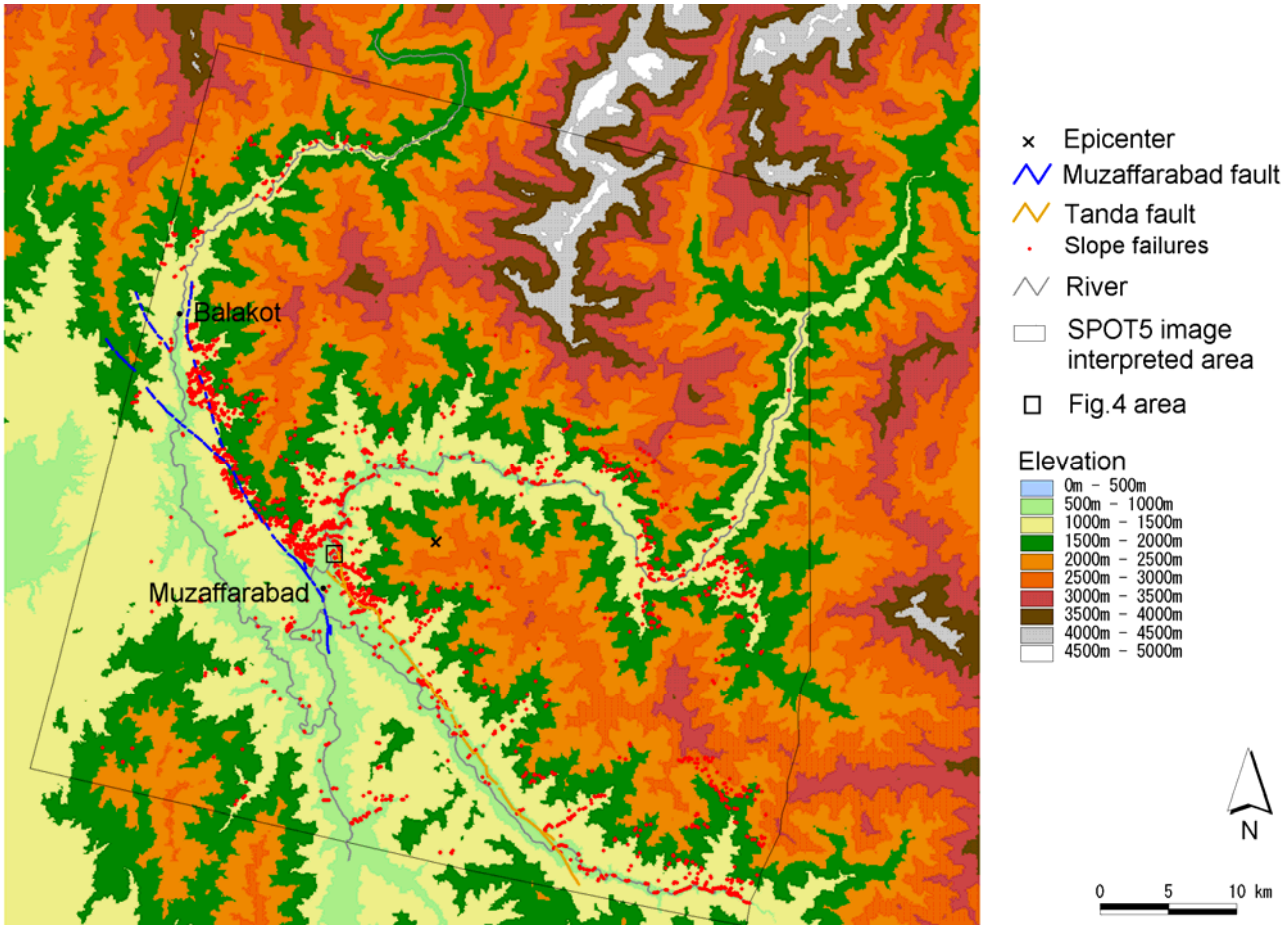

Fig. 5 Distribution of slope failures triggered by the earthquake interpreted using SPOT-5 imagery. Elevation data are based on SRTM.

7. Application of Satellite Data for Disaster Mitigation

For disaster mitigation, two lessons were learned from this study. First, the earthquake occurred on known preexisting active faults. Thus, surveys of existing faults are important for estimating future earthquake hazards and risk. Second, analyses of satellite data can be used to estimate damaged areas for prompt rescue and relief operations because the satellite data show the earthquake faults in detail. From this, relief planners can simulate the seismic damage to effected areas. Perhaps if the displacement field was known immediately after the earthquake, relief operators could have expected that towns close to the earthquake faults such as Muzaffarabad and Balakot would suffer heavy damage.

These results show the importance of satellite data, especially SAR data to the field of hazard and risk management. A problem is that the number of SAR satellites is limited—only ESA's ERS-2 and ENVISAT, and Canada's RADARSAT-1 were in operation in 2005. However, the Japan Aerospace Exploration Agency (JAXA) launched the Advanced Land Observing Satellite (ALOS) on 24 January 2006. ALOS has an L-band SAR sensor, which generally has better coherence (higher signal to noise ratio) than C-band. RADARSAT-2 will be launched later this year.

In addition, distribution map of slope failures is useful to mitigate further disaster. In the monsoon season heavily rain may cause secondary slope failures, and many residents who live on the slope may suffer from the secondary damage of slope failure. To prevent and mitigate such the damage, further monitoring may be important. The interpreted slope failures data will help such disaster prevention measures.

References

Fujiwara, S., Tobita, M., Sato, H.P., Ozawa, S., Une, H., Koarai, M., Nakai, H., Fujiwara, M., Yarai, H., Nishimura, T. and Hayashi, F.: Satellite data gives snapshot of the 2005 Pakistan earthquake, *EOS, Transaction of American Geophysical Union*, 87, 73-77, 2006.

Fujiwara, S., T. Nishimura, M. Murakami, H. Nakagawa, M. Tobita, and P. A. Rosen (2000), 2.5-D surface deformation of M6.1 earthquake near Mt Iwate detected by SAR interferometry, *Geophys. Res. Lett., 27*(14), 2049–2052.

Nakata, T., H. Tsutsumi, S. H. Khan, and R. D. Lawrence (1991), Active faults of Pakistan, 141 pp., Res. Cent. For Reg. Geogr., Hiroshima Univ., Hiroshima, Japan.

Okada, Y. (1985), Surface deformation due to shear and tensile faults in a half-space, *Bull. Seismol. Soc. Am., 75,* 1135–1154.

Tobita, M., M. Murakami, H. Nakagawa, H. Yarai, S. Fujiwara, and P. A. Rosen (2001), 3-D surface deformation of the 2000 Usu eruption measured by matching of SAR images, *Geophys. Res. Lett., 28*(22), 4291–4294.